EFFECT OF BED ROUGHNESS ON THE MIXING LAYERS IN A 90° ASYMMETRICAL CONFLUENCE

STÉPHAN CREËLLE[1], LAURENT SCHINDFESSEL[1] & TOM DE MULDER[1]

(1)   Hydraulics Laboratory, Department of Civil Engineering, Ghent University, Ghent, Belgium
stephan.creelle@ugent.be

ABSTRACT

In this paper, the mixing layer between the two incoming flows in a 90 degree, asymmetrical open channel confluence is investigated. Specific attention is given towards looking into the effect of bed roughness on the flow patterns in the confluence. This analysis is performed in a Serret-Frenet type axis system, in order to come up with a more convenient way of representing the measurement data. The effects on the velocity distribution, velocity difference over the mixing layer, width and location of the mixing layer are studied, and found to be influenced.

Keywords: open channel confluence, mixing layer, hydrodynamics , bed roughness, experiments

1.   INTRODUCTION

Open channel confluences constitute important elements in riverine networks. The complex flow at these confluences is a widely studied topic, since the associated flow features, head losses and mixing properties are of significant importance for the entire network. Because of the high complexity of the 3D flow, and the high number of mutually interacting processes, study of the flow at these confluences requires a suitable simplification of the situation. The conceptual model presented in Figure 1, inspired by the model introduced by Best et al.(1987), is a good starting point, since it allows to delineate different processes within the confluence. One of these important features is the mixing layer between the main and tributary flow. In order to study this mixing layer in a more convenient way, Mignot et al. (2013) proposed the usage of a so-called Serret-Frenet frame-axis.

A Serret-Frenet frame-axis is a type of two-dimensional coordinate system also called a streamline coordinate system or (s,n) system. It uses the local velocity as the direction of the main axis s, i.e. the primary axis s is oriented along the streamlines. The secondary axis, n, is directed along the normal of the streamlines. Hence, a perpendicular frame-axis is obtained.

Adoption of the Serret-Frenet frame-axis explicitly allows to present the flow in the confluence from the viewpoint of the streamline separating from the upstream confluence corner. Although the information in both the Cartesian and the Serret-Frenet frame-axis are equal, the latter facilitates the study of the mixing layer with an increased convenience. Mignot et al. (2013) state that the mixing at a non-parallel, open channel confluence shows comparable features to straight, curved and accelerating mixing layers.

Studies concerning mixing layers are omnipresent, and also bed roughness effects on (shallow) mixing layers have been studied intensively, albeit mostly in the setting of a parallel confluence of two streams separated by a splitter plate. While in those experiments the velocity ratio is identified as the dominant flow forcing, an important effect of bed roughness on the mixing layer properties has been discerned (van Prooijen 2004). In this work, it will be investigated whether similar effects are present in an asymmetrical confluence.
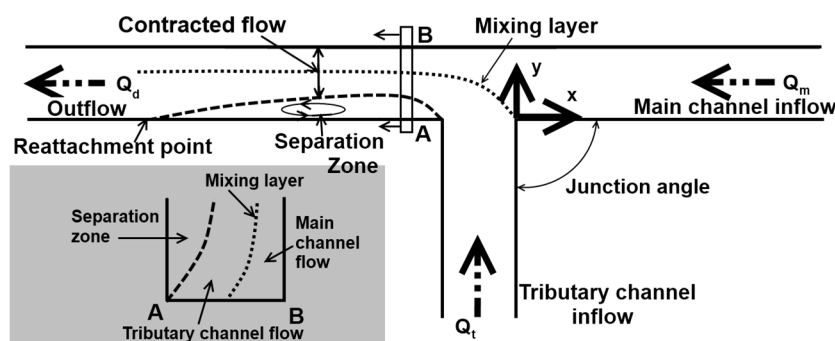

Figure 1 : Conceptual model of confluence flow features

2. OBJECTIVE

The objective of this paper is to investigate the influence of bed roughness on the mixing layer properties at an open channel confluence. In order to look into these properties, it is investigated what influence the bed roughness has on the major parameters used to identify mixing layers in the context of straight mixing layers as studied in literature. These parameters under investigation are the velocity distribution along the normal, the velocity difference over the mixing layer, maximum gradient in and width of the mixing layer. Furthermore, attention is given as to whether the mixing layer and the flow properties in general are different from the flow properties encountered in a parallel mixing layer.

3. EXPERIMENTAL SET-UP

Experiments are performed in an existing flume in the Hydraulics laboratory, consisting of a T-shaped 90°-confluence of two channels having a chamfered rectangular cross-section with concrete walls (Fig. 3). All channels have a fixed, horizontal bed, and have the same width as the downstream channel, namely W_d= 0.98 m. At the upstream boundary of the main and the tributary channels, water is discharged and guided through flow straightening screens, so that a relatively uniform flow is retrieved. As can be seen in Figure 2, after these flow screens, the flow has a length of minimum 20 times the hydraulic radius to adapt to obtain a fully developed flow profile. At the downstream end of the facility, the water level is controlled by means of a weir. Inlet conditions were checked for their uniformity by ADV measurements in a section 1.5W upstream of the confluence. The downstream water depth is 0.415m, induced by the downstream weir.

In order to investigate the effect of roughness on the confluence, two experiments are performed. In the first, the confluence having concrete walls is measured experimentally, as a benchmark case. Thereafter, the roughness is increased by applying artificial grass cover to the bottom and chamfers of the flume. The whole confluence, including the incoming channels, was covered this way. The grass cover was carefully applied, to avoid any discontinuities in the cover.

In both experiments, the total discharge Q_d is 40 l/s, while the flow ratio q=$\frac{Q_t}{Q_d}$=0.75 . This flow ratio is chosen in order to amplify effects of the mixing layer, simplifying the identification of different features. Higher ratios of the flow ratio q were not chosen, since at very high flow ratios the flow behavior at the confluence changes completely, and the overall application of the observed mixing layer behavior would be difficult to generalize (Schindfessel et al., 2014) .

The fixed downstream water level and total discharge, combined with the fixed flow ratio, result in a downstream bulk velocity U_b=0.104 m/s and a Froude number of 0.05 in the downstream branch. Since the head losses over the confluence are negligible considering the low value of Fr_d, this results in a fixed Froude number of 0.04 in the tributary and 0.01 in the upstream part of the main channel. The Reynolds number, based on the (downstream) hydraulic radius, equals Re_d=98000 [-].
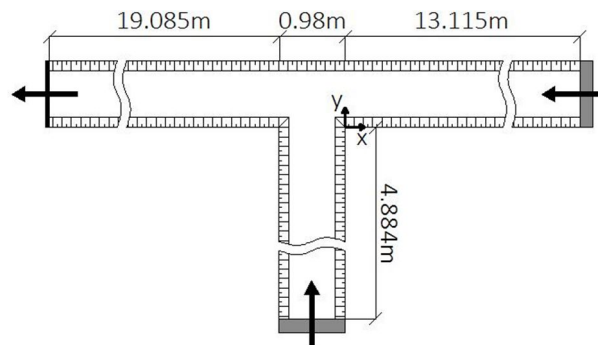

Figure 2 : Experimental flume

Velocity measurements are done with large scale surface particle image velocimetry (LSSPIV). A 1920x1080 pixel camera is used, taking images at a rate of 30Hz. As a seeding material, polypropylene particles are adopted, with a white coating and a maximum size of about 3 mm. The open-source Matlab software package PIV-lab 1.35 (Thielicke 2014) is used for processing the image data into velocity fields.

4. THE SERRET-FRENET FRAME-AXIS

4.1 Introduction of the Serret-Frenet frame-axis

As mentioned in the introduction, the Serret-Frenet frame-axis is a coordinate system based on the streamlines (s-axis) and the normal (n-axis). In order to apply this to the confluence geometry, a clear definition about the origin of the streamlines in necessary. Therefore, the origin will be based on the streamline departing from the upstream confluence corner, i.e. the streamline in the mixing layer, similar to the choice of Mignot et al. (2013). This streamline and the associated coordinate will be denoted with s. Accordingly, the Serret-Frenet frame-axis bounded to this streamline is denoted as the (s,n) coordinate system. The origin of the (s,n) system, s=0, is therefore the start of streamline in the mixing layer. Along the length of the streamline, s will be a decreasing coordinate, whence s<0 in the confluence area and s>0 in the incoming channels.

To determine the Serret-Frenet frame-axis, the streamlines are calculated based on the surface velocity measured with LSSPIV. Since the adopted coordinate system is inherently two-dimensional, some error will be induced at locations where the streamlines are three-dimensional, i.e. where flow dives or surfaces. Note that this error is also present in the measurement technique of LSSPIV, which uses floating particles. Consequently, the chosen coordinate system is suitable to represent the results obtained by the measurement technique applied.

Once the streamlines are found, the normal direction can be calculated easily. The normal are constructed such that they are at every position perpendicular to the local streamwise velocity. The n-axis is positive in the direction away from the centre of curvature. Calculation of the (s,n) coordinates stops at the separation zone, since this would require a separate definition, and this is currently outside the scope of the research.
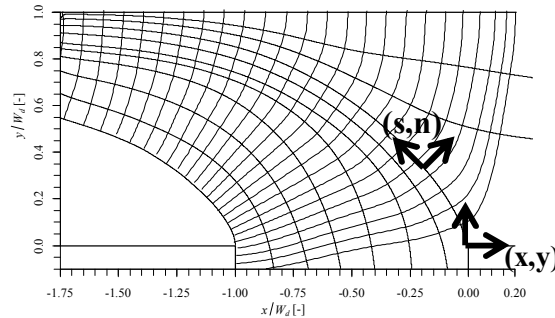

Figure 3 : Definition of the Cartesian (x,y) and Serret-Frenet (s,n) coordinate system

4.2   Cartesian vs. Streamline coordinate system

The objective of this paper is to describe the mechanics of the mixing layer between the main and tributary stream, by looking at the surface velocities, and to investigate whether bed roughness is an influencing parameter for the mechanics of this mixing layer. Earlier work (Uijttewaal 2014, Van Prooijen 2004, Babarutsi et al. 1996 ,Chu et al. 1988) on parallel mixing layers with a velocity difference over a splitter plate has utilized a convenient framework of looking into the velocity difference, the gradient in streamwise velocity over the normal, and to the width of the mixing layer. If the confluence is represented in the (s,n) coordinate system, his allows to have a representation of the flow that can be more easily compared to the framework of parallel mixing layers.

Multiple advantages of this representation are apparent when comparing to the representation in Cartesian coordinates. The flow is represented with reference to the upstream corner, and the streamline separating from that corner. Furthermore, the discontinuous geometry that looks artificial, is replaced by the geometry of the flow itself. This is interesting, since the geometry changes together with the flow, as the hydraulic boundary conditions in the confluence change . The contraction of the free stream section also becomes clearly pronounced, as is the portion of the free stream path taken by both the flow coming from the main channel and the tributary. However, information about the curvature of the streamlines becomes hidden, and information of the separation zone vanished, since this flow is detached from the flow in the confluence itself.

5.   RESULTS

5.1   Validation of LSSPIV measurements

As described in section 3, LSSPIV is applied to obtain the velocity fields at the flow surface. Application of the technique in the context of the 90° confluence under consideration is however not trivial. Since the technique works with floating tracers, and the flow is highly three-dimensional, obtaining a well seeded flow proves difficult, especially in zones where vertical velocities are present, resulting in either clogging of the tracers or zones with a sparse or no seeding. The separation zone in particular seemed to be an area leading to difficulties of seeding, because of the large time-dependent structures that exist over there.

In order to establish the reliability of the technique to obtain surface velocities, two near-surface velocity profiles are measured by a Nortek Vectrino II ADVP (in the sweet spot), and compared in Figure 4. The velocities presented are measured at a cross-section at the location x/W=-0.5W .
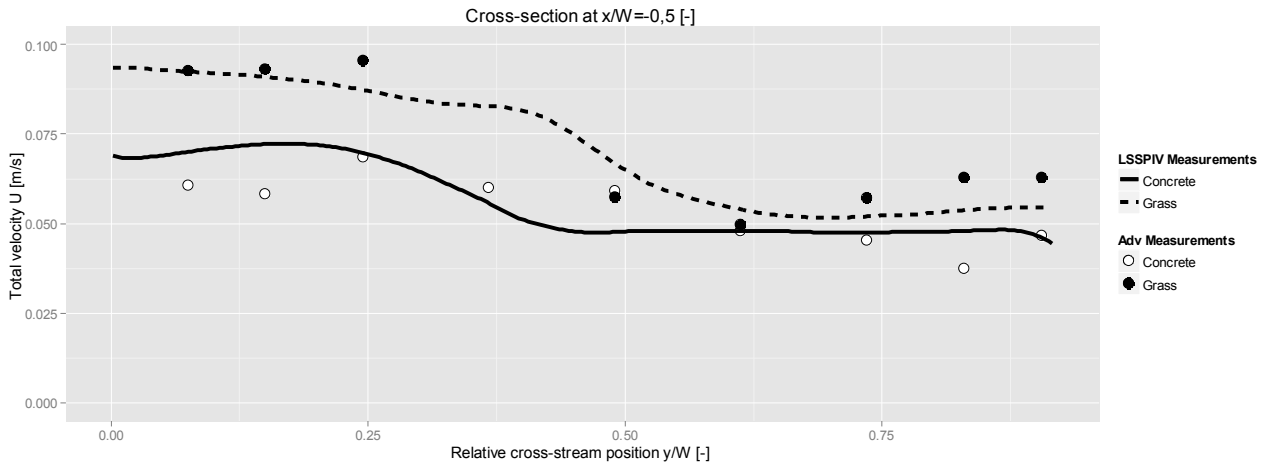
Figure 4 : Comparison of LSSPIV and ADV measurements

Although some discrepancies can be seen, the general profile of the flow is captured. Moreover, it is important to remark that the measurements with the ADV are taken at about 2 cm below the free surface, since no measurements can be made at the surface.

5.2 Velocity fields

Recorded velocity fields are presented in Figure 5. The area of interest is chosen to cover the confluence area, up to the point where the separation zone has reached its maximum width. The measurements also cover a certain distance area upstream of the confluence, both in the main channel and in the tributary. This is done to make sure the normal starting close to the point of flow stagnation can be calculated in full, in order to cover the inflow conditions as such.
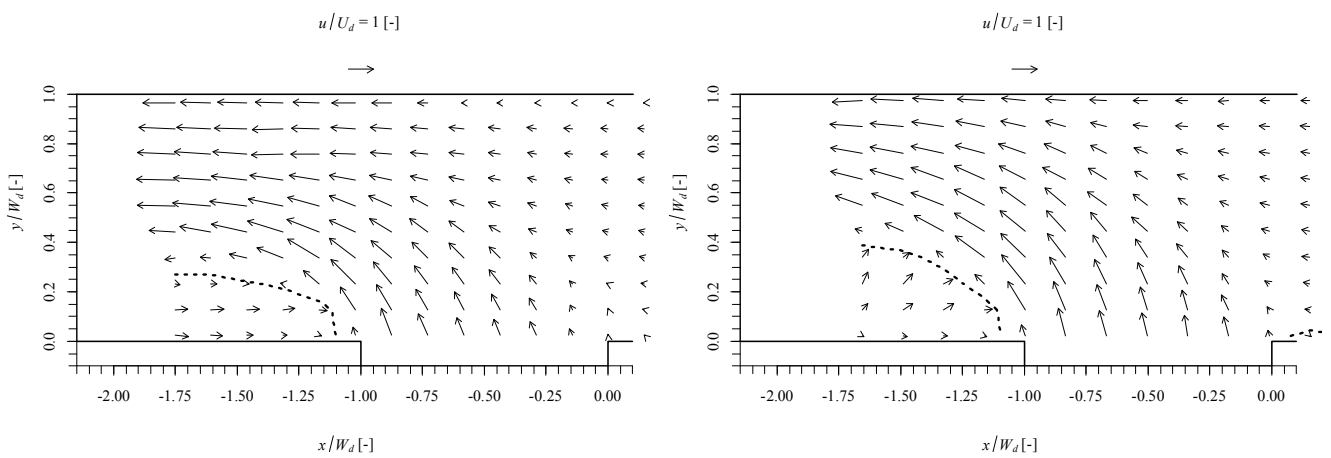

Figure 5 : Surface velocities measured by LSSPIV: (left) Concrete bottom; (right) Grass bottom

The general flow features identified in Figure 1 are clearly visible. The mixing layer stretching from the stagnation point at the upstream corner into the confluence. The intense shear layer between the separation zone and the tributary flow is also clearly discernible. Identification of differences between the concrete and grass bed case from these arrow graphs proves difficult, although some small differences can be distinguished. First of all, the zone with upstream velocities (indicated by the dotted contour line) is somewhat wider in the case with the grass cover. Secondly, in the case with the grass cover, the flow is pointed more towards the outer bank, which can be seen as the cause of the wider zone of upstream velocities, since the flow from the tributary protrudes further into the main channel. It is noted that the velocity profile of the incoming discharge from the tributary shows a maximum at the downstream corner, and becomes smaller towards the upstream corner.
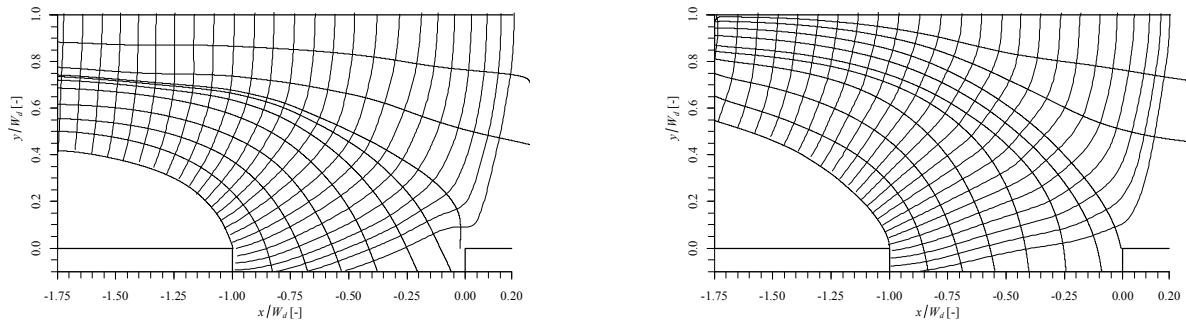
Figure 6 : Streamlines and normals in the confluence: (left) Concrete bottom; (right) Grass bottom

In Figure 6 some streamlines and normals are drawn in the confluence area. It is clear that the streamline starting at the downstream corner, delineating the zone of flow separation, penetrates further into the confluence, thus effectively widening the width of the separation zone. The decreased free stream width for the flow coming from the main channel can also be seen quite clearly. At the entrance section of the tributary channel into the confluence, a clear curvature of the streamlines can be seen, with a stronger curvature at the downstream corner, and with decreasing curvature towards the upstream corner. These results are interesting when comparing it to the ideal confluence shape as derived by Webber & Greated (1966). The flow forms its own flow geometry within the physical boundaries imposed by the channel banks, and shows resemblances to the ideal confluence geometry derived in their work.

5.3 Evolution of the velocity profiles over the confluence

Investigating the mixing behavior of the flow incoming from the inlet channels towards downstream, requires to look into the evolution of the velocity profiles along the mixing layer. In Figure 7 some velocity profiles along a normal are represented, illustrating how the velocity profiles imposed at the upstream boundaries of the confluence evolve into the profile at the most contracted section in the confluence.

It is clear that the initial velocity difference between the incoming flow, imposed by the flow ratio q and the fact that head losses over the confluence are negligible, is quickly reduced along the mixing layer. Quantification of the velocity difference in this case proves however less straightforward than in parallel confluences. While at the side of the main channel a clearly distinguishable bulk velocity of the flow can be identified, the velocity at the side of the tributary shows no clear bulk velocity. Instead, the velocity is steadily increasing with increasing distance from the separating streamline. This observation was also already made earlier, where it was noticed that the highest velocities are situated at the downstream corner.

In order to quantify the velocity difference, a representative velocity of the flow from the tributary side (U_t) and main channel side (U_m) have to be defined. Although no clear bulk velocity can be observed in the tributary flow, the inflexion in the velocity profile, associated with a horizontal mixing layer is clearly discernable.

Therefore it is chosen to locate the bulk velocities, by looking at the gradient of the velocities over the normal direction. The reference velocities are chosen at the local maxima, in the vicinity of the mixing layer. This gradient is also shown in Figure 7 with a line, at the bottom of the figures. The associated reference velocities are also indicated in the plots. In the last section presented, the velocity difference and its associated inflection point are hardly discernible anymore. This is caused by the fact that the velocity difference over the mixing layer has become very small, and that the shear layer from the separation zone is becoming more and more spread over the normal, and becoming the most significant influence on the velocity profile.
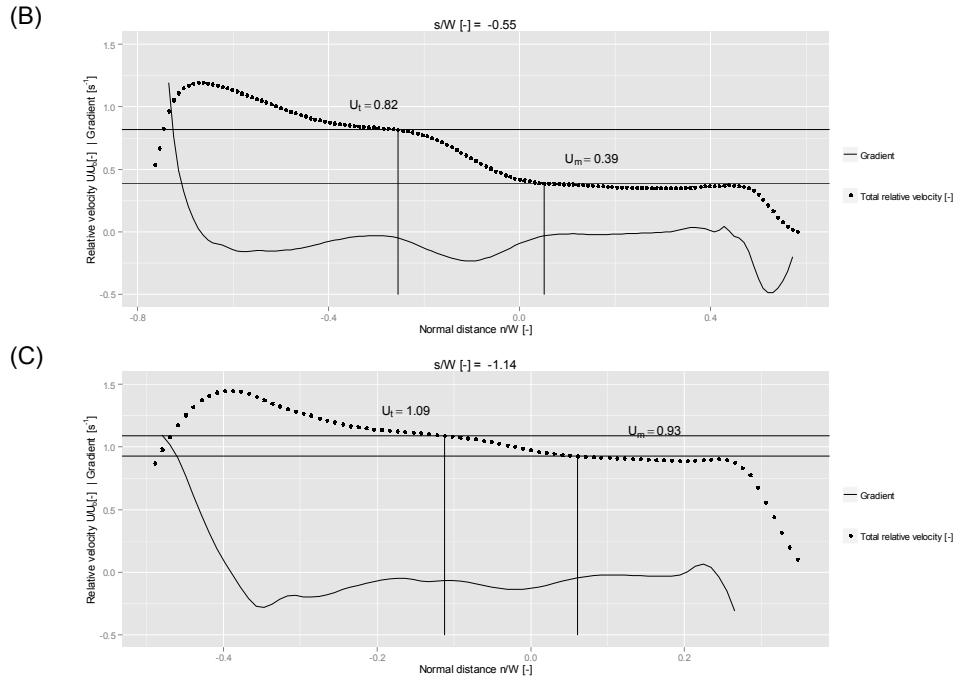
(A)

(B)

(C)
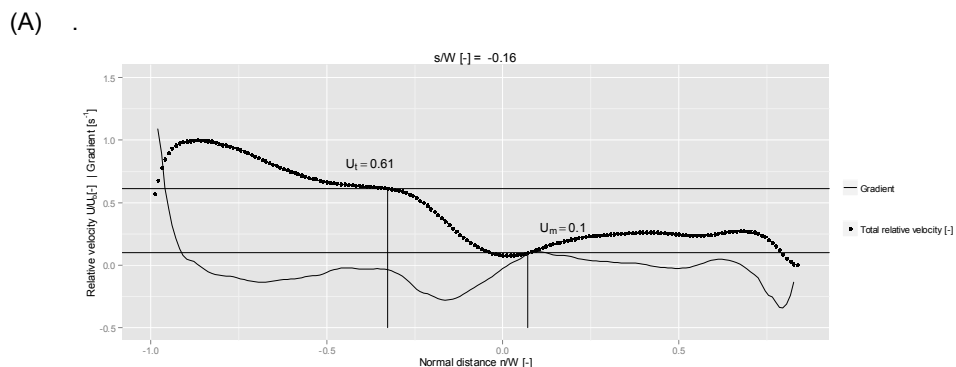
Figure 7 : Velocity profiles along a normal: (A) at s/W=-0.16; (B) at s/W=-0.55; (C) at s/W=-1.14

It is noticed that for both cases the inflection point in the velocity profile is lying somewhat to the tributary side of the separating streamline. This observation is consistent with findings by Mignot et al. (2013) who also find that this point lies at the side of the branch subjected to the highest flow. This is a notable difference with parallel (plane) mixing layers, where the inflection point is shifted to the low velocity side of the mixing layer (van Prooijen 2004).

5.4   Width of free stream paths

Because of the development of the separation zone, a flow contraction takes place. The available free stream path is narrowed, and flow has to accelerate next to the separation zone. The width of the total free stream path is plotted in Figure 8. Remember this is the distance measured along the normal, thus it is a somewhat different definition than what in literature is defined as the free stream path, measured normal to the side walls. This also makes that the width of the separation zone cannot be calculated as the width of the section minus the free steam path, as is often done in the Cartesian frame axis.

As indicated in paragraph 5.2, the change in bed roughness has changed the velocity field at the free surface. The trajectory of the streamline starting at the upstream corner is altered, resulting in a difference in the widths of the flow sections available for the flow from the main channel and tributary. The evolution of the width (measured along the normal), available for the flow, is represented in Figure 8. The additional bed roughness results in a larger width available for the tributary flow when compared to the smooth bed case.
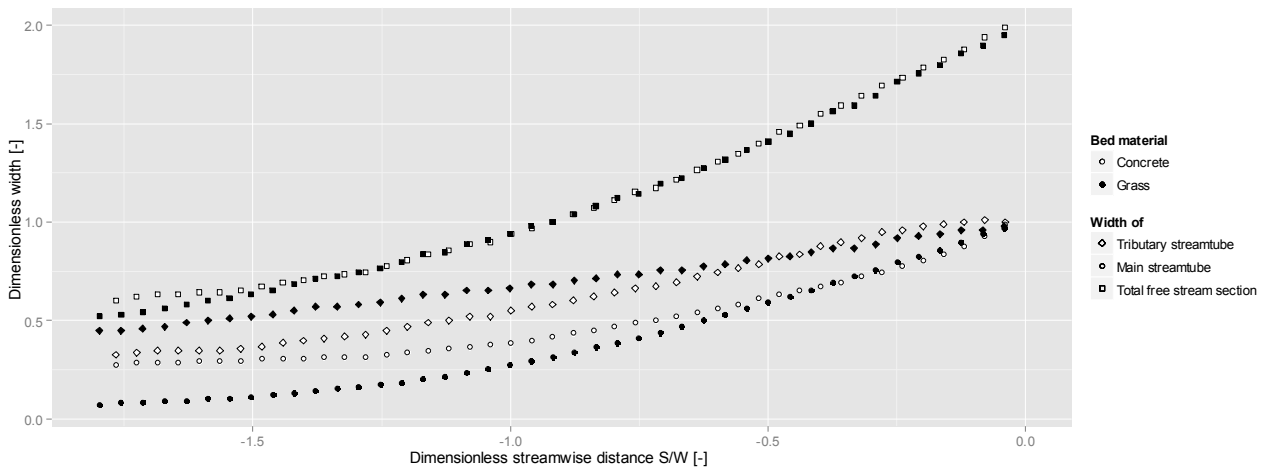

Figure 8 : Width of the stream tubes

For both the smooth (concrete walls) and rough conditions (grass cover), the available width for flow from the tributary is higher than for the flow from the main channel. Far enough upstream of the confluence the velocity normals are perpendicular to the side walls, and the available width for both is W. The combined available width is thus two times the channel width W. In the confluence region, the available total width is quickly reduced to W. Moreover, because of the lateral momentum content of the tributary flow, the formation of the separation zone (locally) further reduces the available freestream section. It can also be seen that the part of the free stream section occupied by flow from the tributary occupies a larger portion.

This should not be surprising, given that the flow from the tributary carries three times more flow than the main channel in case of q=0.75. However, the width available for the main channel flow is not three times as small, and thus relatively to the flow it is carrying, it is wider. This can be seen in Figure 7, where the velocities in the tributary are larger than those coming from the main channel.

5.5   Velocity difference over the mixing layer

As explained in the previous paragraph, and can be seen in the profiles presented in Figure 7, a velocity difference between the inflowing branches exists. It is important to see that this velocity difference over the mixing layer is not solely defined by the flow ratio, because of the redistribution of the flow over the available flow section.

With the procedure as explained in paragraph 5.3, the representative bulk velocities $U_m(s)$ and $U_t(s)$ can be defined, and the velocity difference over the confluence can be calculated, both for the smooth and rough bed case.

Figure 9 : Evolution of velocities along the streamline

Results in Figure 9 clearly show that both sides of the mixing layer are quickly accelerating, caused by the rapid contraction of the freestream width. In order to be able to assess the influence of this contraction of the stream paths, a reference velocity magnitude is presented. This velocity magnitude is obtained by dividing the channel width by the locally available stream width.

In both the smooth and rough bed case the flow in the main accelerates faster than the flow from the main channel, reducing the velocity difference as such. It can also be seen that in both cases the velocities in both flow regions drop below the reference velocity. This means that flow rate per unit height is relatively lower than in the rest of the flow. This is indeed in accordance with other observations (e.g Shumate 1998) that observed that the zone of flow separation is widest at the top, and is smaller closer to the bottom.

Furthermore it shows that the velocity difference in both configurations is decaying as a function of the streamline coordinate, as can be expected. At this instance it is recalled that the experiments were performed at a flow ratio q=0.75. Therefore, far enough upstream the velocities in the tributary are three times higher than those in the upstream part of the main channel. At the beginning of the mixing layer, this indeed holds about true, although some effect of the redistribution can be seen. Figure 10 shows the velocity difference as a function of the distance along the streamline. Despite the difference in magnitude of the velocities between the cases, the velocity difference features a similar evolution in both cases.
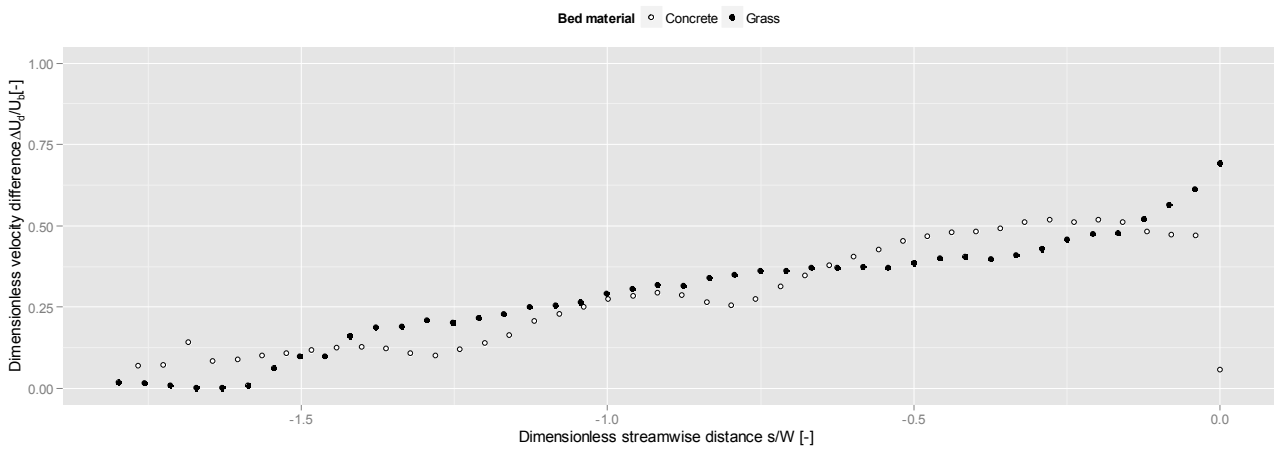
Figure 10 : Velocity difference over the mixing layer
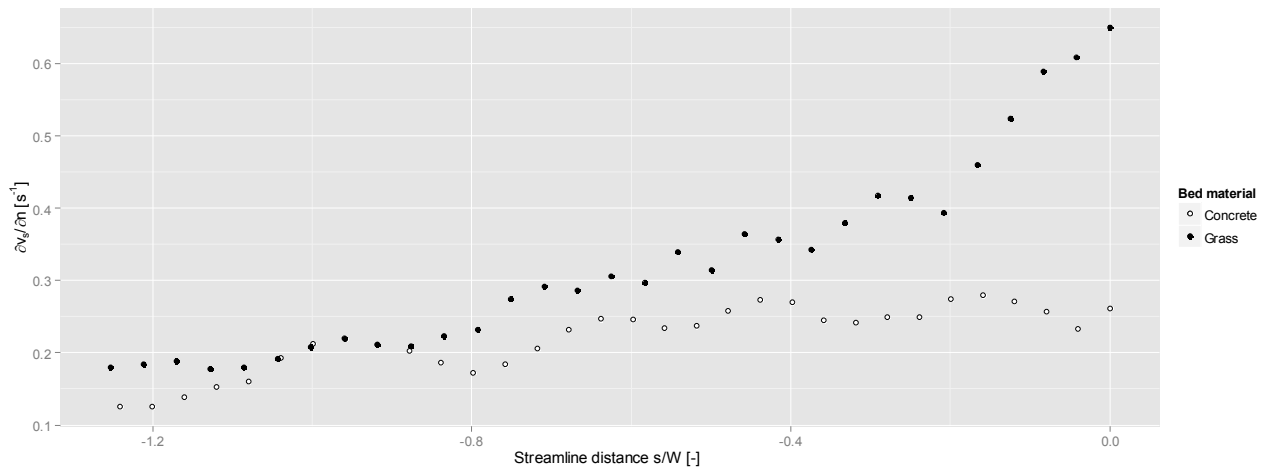
5.6 Maximum normal velocity gradient

Figure 11 : Evolution of the maximum normal gradient of streamwise velocity

Figure 11 shows the evolution of the maximum normal velocity gradient, both for smooth and rough bed conditions. It is observed that the initial gradient is larger for the rough bed case, and is decreasing faster. The higher initial difference might be caused by the fact that the bed roughness is reducing the flow redistribution upstream of the confluence, although further investigation is needed to identify the cause for this observation.

5.7 Mixing layer width

In literature of parallel mixing layers, the width of the mixing layer is classically defined as

$$\delta(s) = \frac{\Delta U(s)}{|\frac{\partial \overline{u_s}}{\partial n}|_{max}} \qquad [1]$$

Figure 12 shows the evolution of the width of the mixing layer for both cases. It can be seen that for the case of the concrete bed, the width of the mixing layer is steadily decreasing, while for the case of the grass bed cover the mixing layer width is smaller, and stays more or less equally wide.
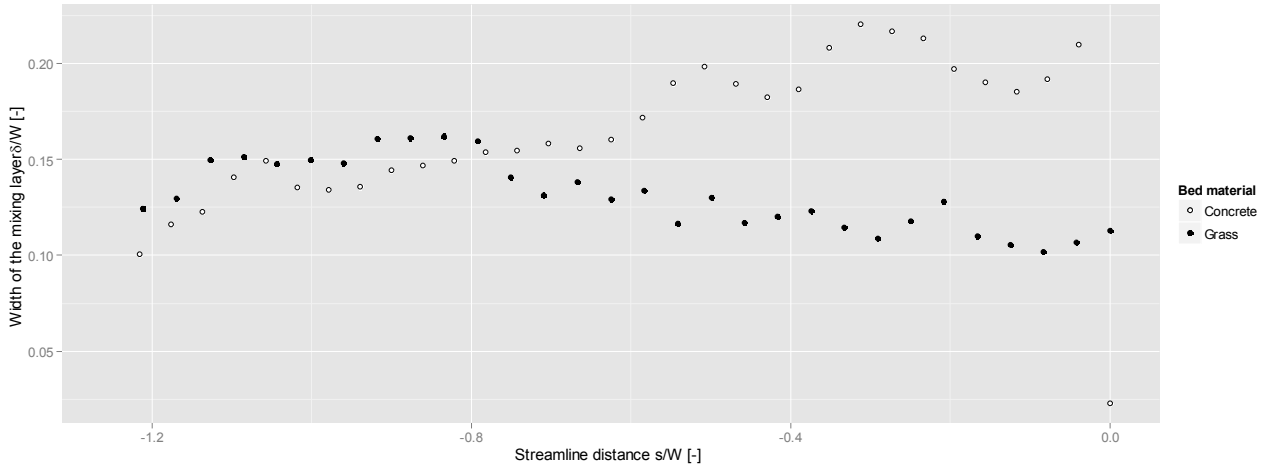
Figure 12 : Width of the mixing layer

An alternative definition of the width of the mixing layer could be found by calculating the distance between the points where the reference velocity is calculated in paragraph 5.3. While the velocity difference over this distance is the same, the gradient is now the average gradient over the mixing width. Therefore this alternative definition leads to the larger values of the width of the mixing layer presented in Figure 13.
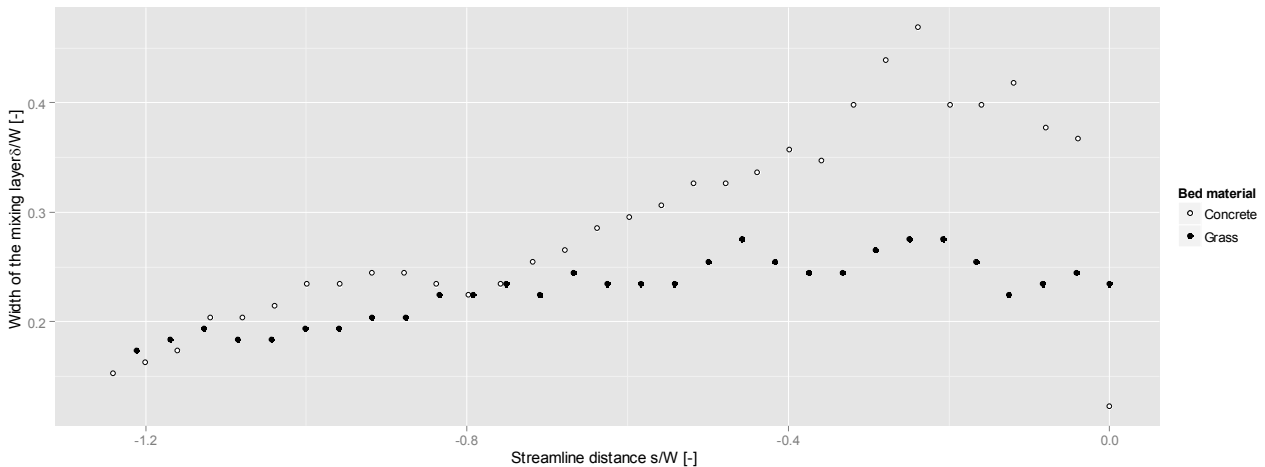

Figure 13 : Width of the mixing layer (distance between local normal gradient maxima)

The trend for the smooth bed case remains unchanged, with a steady decrease from a certain value . For the rough bed case, a slight decrease in width in the downstream direction is observed, opposed to the constant width observed in Figure 12.

6. DISCUSSION

Investigation of the flow in an open channel confluence, by use of a transformation to a (s,n) frame axis has proven to provide with a new representation of the velocity field and its associated flow features. Some precaution has to be taken however, since the transformation is dependent on the location of the streamline starting at the upstream corner. Flow velocities at this corner are very close to zero, since it coincides with the flow stagnation zone. Therefore from a practical viewpoint, when calculating the separating streamline from the experimental data, a point somewhat removed from the physical corner has to be chosen. It has been confirmed that the choice of the location of this point is not significantly influencing the results and conclusions in this paper. This can be seen intuitively as well, as the streamlines close to the separation zone are contracting very fast when moving away of the point of flow stagnation, since very little flow is flowing through this zone of flow stagnation. However, more measurements and research have to be performed prior to generalizing the results obtained in this study, since some of the parameters are based on derivatives of measured quantities, and thus are sensitive to measurement inaccuracies.

As discussed in section 5, identifying the inflection point in the velocity profile and the associated bulk velocities becomes increasingly difficult for increasing distance into the confluence. This is an expected result when comparing to parallel mixing layers, because the velocity difference becomes smaller. In the context of these non-parallel confluences, a second factor is however of even larger importance, namely the shear layer between the flow in the tributary stream tube and the flow in the separation zone. Flow velocities at the downstream corner of the confluence have been identified to have the largest magnitude. In the zone of flow separation however, even upstream oriented flow is encountered, when looking close to the wall. This makes that the velocity difference over this shear layer is very large compared to the velocity

difference over the mixing layer. While the maximum velocity difference over the mixing layer has shown to be in the order of 50% of the bulk velocity, the velocity difference over the shear layer can go up to 150-200%. This goes along with a high streamwise momentum deficiency in and downstream of the separation zone, that has to be filled by lateral transport of streamwise momentum. Earlier numerical work has shown that bed roughness can play an influencing role in this redistribution of streamwise momentum to the lee of the separation zone (Creelle et al.,2014).

It has to be noticed that the analysis of the flow behavior concerning the mixing layer has been looked upon from a time averaged perspective. Time dependent coherent structures are however an important element of the flow behavior of this mixing layer. While time-averaged effects of these coherent structures are incorporated in the time-averaged data, the temporal behavior of the mixing layer has not been discussed. Visual observations from the measurements show that indeed coherent structures emerge in the mixing layer, and are transported downstream. Furthermore it is observed that the location of the mixing layer seems to be fluctuating, and is not fixed in time.
Coherent structures are also shed from the downstream corner, where the shear layer separating the flow from the tributary and the separation zone is very intense. These structures are much higher in number and shedding frequency and seem to grow faster than the ones in the mixing layer. This can be understood as the velocity difference causing them is far more pronounced. These fast growing structures are observed to reach dimensions in the order of half the width of the channel in a short distance, and they start interacting with the structures in the mixing layer. More investigation in both these sources of coherent structures, their growth, interaction and decay downstream of the confluence is surely something interesting to investigate further.

7. CONCLUSIONS

In this paper, the mixing layer at the interface between the two incoming flows in a 90° open channel confluence has been studied. In general, it has been found that the application of the Serret-Frenet frame axis as introduced in Mignot et al. (2013) serves as a convenient way of representation of the flow dynamics in the confluence. With the aid of an LSSPIV technique, velocities at the water surface were recorded.

In general, flow quantities identified in the context of a parallel confluence can be related with the behavior of the mixing layer of an asymmetrical confluence. The incoming streams impose an initial velocity difference over the mixing layer that is gradually fading out when going further downstream, and clear inflection point in the velocity profile can be observed. However, when compared to the mixing layer in a parallel confluence, some important differences are present. First of all the total available section over the confluence is reduced from two times the channel width to a single channel width. Furthermore, the lateral momentum from the tributary channel causes the formation of the separation zone. This separation zone, together with the physical confinement of the channel walls, subjects the flow to a complex confinement of the available flow area. Acceleration of the total flow is caused by this confinement, and it intensifies the uniformisation of the velocities between the flow from the main channel and the tributary.

By running additional experiments with an artificial grass cover applied to the bed, differences caused by an increase in bed roughness have been recorded. The increase in bed roughness changed the streampath of the streamline separating the flow from the tributary and the main channel. Additionally, a larger initial velocity gradient is established by the increased bed roughness. Increase in bed roughness seems to have little effect on the rate of uniformisation of the flow, since the velocity difference is decaying equally fast in both cases. The width of the mixing layer however seems to be slightly smaller in the case of the rough bed.

Because of the complex confinement of the flow, and the high degree of asymmetry in the confluence geometry, the velocity profile of the incoming flows is also changed up to a certain distance upstream of the confluence. Especially the redistribution in the tributary flow is significant, with high velocities at the downstream corner, and lower velocities at the upstream corner. This observation is in line with earlier observations of (Weber et al. 2001, Hsu et al. 1998, Ramamurthy 1988) of the flow at the tributary inflow section of an assymetrical confluence.

Besides the mixing layer, a shear layer with an even larger velocity difference is formed at the downstream corner, between the highly accelerated flow at downstream wall of the tributary and the separation zone. The influence of this shear layer is quickly growing, and starts interacting with an already highly attenuated mixing layer by the time it arrives in the section of the downsteam corner. Therefore once the effects of the shear layer start interacting with the ones of the mixing layer, the mixing layer can hardly be distinguished anymore.

Visual observations during the experiments reveal horizontal coherent structures shedding from both the upstream and downstream corner. As can be expected from the velocity differences, the intensity and size of the ones at the upstream corner, traveling in the mixing layer, are smaller than those shedding from the downstream corner, traveling near the shear layer. The interaction of both types of coherent structures and their downstream evolution is an interesting topic for further investigation.

ACKNOWLEDGMENTS

REFERENCES

Babarutsi, S., Nassiri, M., & Chu, V. (1996). Computation of Shallow Recirculating Flow Dominated by Friction. *Journal of Hydraulic Engineering, 122*(7), 367-372. doi: doi:10.1061.

Best, J.L., (1987.) Flow Dynamics at River Channel Confluences: Implications for Sediment Transport and Bed Morphology. *Recent Development in Fluvial Sedimentology*, Ed. F.G. Etheidge, R.M. Flores and M.D. Harvey . SEMP Spec. Publishers, UK., pp: 27-35.

Creëlle S., De Mulder T., Schindfessel L. and Van Oyen T. (2014). Influence of hydraulic resistance on flow features in an open channel confluence. 3rd IAHR Europe Congress, Ed. de Almeida et al., Porto, 10 pp.

Chu, V., & Babarutsi, S. (1988). Confinement and Bed Friction Effects in Shallow Turbulent Mixing Layers. *Journal of Hydraulic Engineering,* 114(10), 1257-1274. doi: doi:10.1061.

Hsu, Wu, F., & Lee. (1998). Flow at 90° Equal-Width Open-Channel Junction. *Journal of Hydraulic Engineering, 124*(2), 186-191. doi: doi:10.1061

Mignot, E., Vinkovic, I., Doppler, D., & Riviere, N. (2014). Mixing layer in open-channel junction flows. *Environmental Fluid Mechanics, 14* (5) , 1027-1041.

Ramamurthy, A., Carballada, L., & Tran, D. (1988). Combining Open Channel Flow at Right Angled Junctions. *Journal of Hydraulic Engineering, 114*(12), 1449-1460. doi: 10.1061

Schindfessel, L., Creëlle, S., Boelens, T., & Mulder, T. D. (2014). Flow patterns in an open channel confluence with a small ratio of main channel to tributary discharge. *River Flow 2014* , CRC Press.,989-996.

Shumate, E. D. (1998). Experimental description of flow at an open-channel junction. Master thesis. Univ. of Iowa. Iowa.

Thielicke, W. and Stamhuis, E. J. (2014): PIVlab - Time-Resolved Digital Particle Image Velocimetry Tool for MATLAB (version:1.35).http://dx.doi.org/10.6084/m9.figshare.1092508.

Uijttewaal, W. S. J. (2014). Hydrodynamics of shallow flows: application to rivers. *Journal of Hydraulic Research, 52*(2), 157-172. doi: 10.1080/00221686.2014.905505.

Van Prooijen, B. (2004). *Shallow mixing layers.* TU Delft, Delft University of Technology.

Webber, N. B., & Greated, C. (1966). An investigation of flow behaviour at the junction of rectangular channels. Paper presented at the ICE Proceedings.

Weber, L., Schumate, E., & Mawer, N. (2001). Experiments on Flow at a 90° Open-Channel Junction. *Journal of Hydraulic Engineering, 127*(5), 340-350. doi: doi:10.1061.